

## Production of nuclides near the $N = 126$ shell in $^{48}\text{Ca}$ , $^{50}\text{Ti}$ , and $^{54}\text{Cr}$ induced reactions

D.A. Mayorov, T.A. Werke, M.C. Alfonso, M.E. Bennett, and C.M. Folden III

Modern theoretical calculations conclude that the most promising reaction pathway to the synthesis of elements heavier than 118 is fusion of  $^{50}\text{Ti}$  with actinides [1]. At present, the low intensities of necessary beams in alternative production mechanisms (i.e. neutron-rich radioactive beams, low energy damped multi-nucleon transfer) make them inferior to “hot” fusion [2]. However, despite being most promising, the estimated cross sections for synthesis of element 120 in the  $^{50}\text{Ti} + ^{249}\text{Cf}$  reaction are on the order of tens to hundreds of femtobarns, much lower than the picobarn-level observed for a number of its immediate lighter predecessors. The reduction in projectile-target asymmetry in the  $^{50}\text{Ti}$  reaction, relative to the  $^{48}\text{Ca} + ^{249}\text{Cf}$  fusion, and, possibly (likewise surprisingly), the proximity of its product to the predicted proton and neutron shell closures of the island of stability can be linked to this low prediction.

A series of reaction systems, with significantly higher product yield than the case of superheavy elements, were chosen for a study to better quantify the role the projectile plays on the reaction cross section (specifically a relative comparison among  $^{48}\text{Ca}$ ,  $^{50}\text{Ti}$ , and  $^{54}\text{Cr}$ ). Table I summarizes these and draws attention to the systems explored to date (shown in bold). Furthermore, the reaction systems all produce residues in the vicinity of the  $N = 126$  shell closure; the next closed neutron shell is predicted at  $N = 184$  and is being approached with the search for element 120 [3]. This aids in determining the effect of the shell correction energy on the survival probability of the residue.

**Table I.** Comparison of reactions of interest in the current work. Data for the items in bold are presented in this report. Column 2 features a measure of the reaction projectile-target pair mass asymmetry. Values of the ground-state (equilibrium) quadrupole deformation, column 3, are taken from [13]. Fission barriers ( $B_f$ ) are calculated according to [14] and neutron binding energies ( $B_n$ ) are based on ground-state masses from [15].

Reaction $A_p + A_T \rightarrow A_{CN}$	$\eta = \frac{ A_p - A_T }{A_p + A_T}$	$\beta_{2,CN}^{eq}$	$[B_f - B_n]_{CN - to - 3n}$ (MeV)
$^{48}\text{Ca} + ^{159}\text{Tb} \rightarrow ^{207}\text{At}$	0.536	-0.035	7.20, 7.65, 4.71, 5.42
$^{48}\text{Ca} + ^{162}\text{Dy} \rightarrow ^{210}\text{Rn}$	<b>0.543</b>	<b>-0.026</b>	<b>7.05, 7.50, 4.79, 5.49</b>
$^{48}\text{Ca} + ^{165}\text{Ho} \rightarrow ^{213}\text{Fr}$	0.549	0.008	6.81, 7.27, 4.83, 5.19
$^{50}\text{Ti} + ^{159}\text{Tb} \rightarrow ^{209}\text{Fr}$	<b>0.522</b>	<b>-0.044</b>	<b>2.75, 3.27, 0.69, 1.59</b>
$^{50}\text{Ti} + ^{162}\text{Dy} \rightarrow ^{212}\text{Ra}$	0.528	-0.035	2.68, 3.25, 0.57, 1.49
$^{50}\text{Ti} + ^{165}\text{Ho} \rightarrow ^{215}\text{Ac}$	0.535	0.000	2.70, 3.13, 0.76, 1.17
$^{54}\text{Cr} + ^{159}\text{Tb} \rightarrow ^{213}\text{Ac}$	0.493	-0.044	0.76, 1.17, -1.29, -0.27
$^{54}\text{Cr} + ^{162}\text{Dy} \rightarrow ^{216}\text{Th}$	<b>0.500</b>	<b>0.008</b>	<b>0.84, 1.45, -1.11, -0.34</b>
$^{54}\text{Cr} + ^{165}\text{Ho} \rightarrow ^{219}\text{Pa}$	0.507	-0.008	-1.73, 0.80, -0.78, -0.37

Fig. 1 shows the preliminary measured excitation function for the ( $^{48}\text{Ca}$ ,  $4n$ ) reaction and the upper limits for the ( $^{54}\text{Cr}$ ,  $4n$ ) reaction on a  $^{162}\text{Dy}$  target, with the experimental set-up details identical to

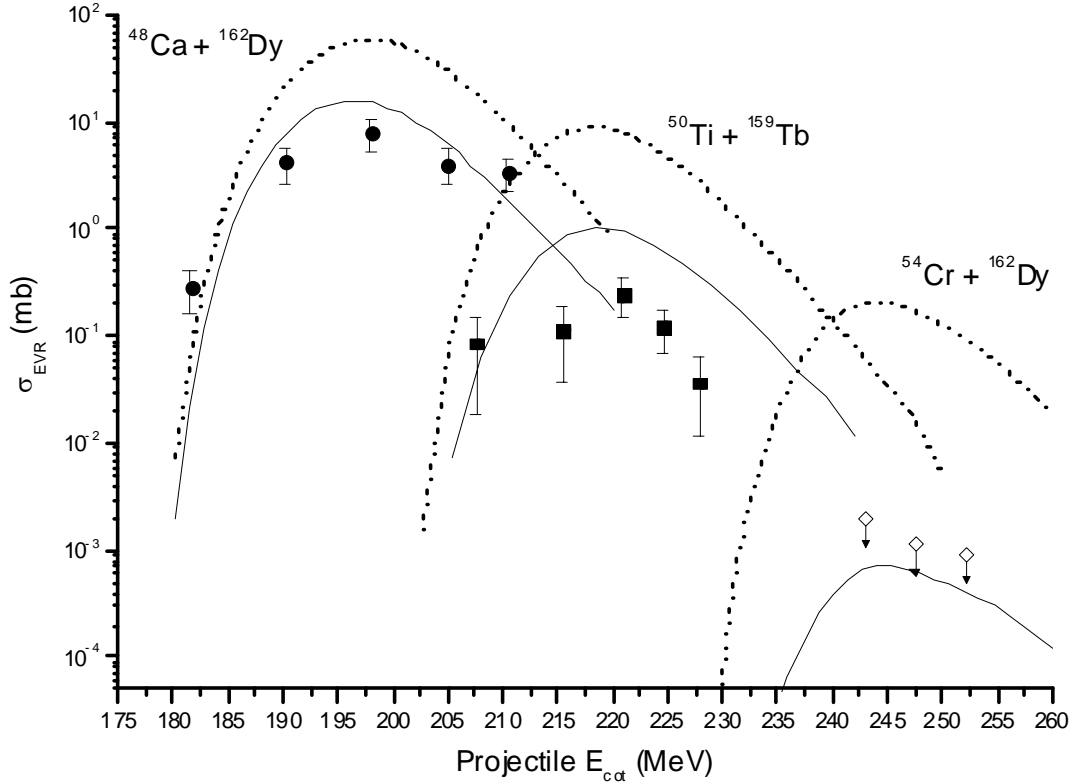


**FIG. 1.** Excitation functions for  $^{162}\text{Dy}(^{48}\text{Ca}, 4n)^{206}\text{Rn}$  (circles),  $^{159}\text{Tb}(^{50}\text{Ti}, 4n)^{205}\text{Fr}$  (squares), and  $^{162}\text{Dy}(^{54}\text{Cr}, 4n)^{212}\text{Th}$  (diamonds). Upper limits for  $^{212}\text{Th}$  are calculated with an 84% confidence interval according to [16]. A factor of over 7300 separates the  $4n$  reaction products for the reactions involving  $^{162}\text{Dy}$  target. Solid and dashed curves are theoretical calculations, with a distinction that the dashed curves exclude collective enhancements in the calculation [6].

those described in [4] (also see [5]). In addition, the most recent data from the  $(^{50}\text{Ti}, 4n)$  reaction on  $^{159}\text{Tb}$  is included for comparison. The dashed and solid curves are theoretical calculations based on the models of Zagrebaev et al. [6], with the distinction of the latter accounting for collective enhancements. Vermulen et al. [7] previously observed reduced survival probabilities of nuclides produced via fusion-evaporation near the  $N = 126$  shell closure. This phenomenon was later explained by expanding the energy level density of the potential de-excitation modes of a “hot”, rotating compound nucleus to include collective nucleon excitations. In cases of weak nuclear deformation, the contribution from rotational excitation heavily favors the fission channel, meanwhile the contribution for the  $xn$  channels is at least an order of magnitude smaller [6, 8].

The much lower production cross section for  $^{162}\text{Dy}(^{54}\text{Cr}, 4n)^{212}\text{Th}$  compared to  $^{162}\text{Dy}(^{48}\text{Ca}, 4n)^{206}\text{Rn}$  is best explained by referring to column 4 of Table I, which summarizes for each respective compound nucleus the barriers encountered along the de-excitation cascade for the two primary decay modes of fission and neutron emission up to the  $3n$  intermediate, which then leads to the  $4n$  ground-state residue. Fission dominates for the heavier residue, suppressing its survival probability. In addition, the falling survival probability increasingly augments the magnitude of the effect from collective

enhancements as seen from the calculated solid curves from left to right in Fig. 1 [6]. This can be attributed to the growing magnitude of the product between a calculated enhancements factor and quickly rising fission probability for the heavier residues, which shifts the de-excitation in favor of fission.

Another key feature in Fig. 1 is the gap observed between the experimental points and the theoretical predictions (solid curves, which assume that probability of compound nucleus formation is unity [9]). This difference corresponds to the probability of complete fusion following projectile-target collision; the competing process is quasi-fission after collision resulting in re-separation of the nuclei before overcoming the saddle point. Preliminary analysis based on the approach employed in [10] suggests that the fusion probability (also probability of compound nucleus formation) falls from 0.50 to 0.25 to 0.10, for the  $^{48}\text{Ca}$  to  $^{50}\text{Ti}$  to  $^{54}\text{Cr}$  reactions, respectively, at the maximum of each excitation function. An estimate for the peak cross section in the case of  $^{162}\text{Dy}(^{54}\text{Cr}, 4n)^{212}\text{Th}$  was based on literature data for reactions with greater and lesser  $\eta$  (as defined in Table I), and forming the same compound nucleus and residue [7, 11]. These are  $^{176}\text{Hf}(^{40}\text{Ar}, 4n)^{212}\text{Th}$ ,  $^{154}\text{Sm}(^{68}\text{Ni}, 4n)^{212}\text{Th}$ , and  $^{92}\text{Zr}(^{124}\text{Sn}, 4n)^{212}\text{Th}$ , all of which cluster at  $\approx 100$  nb for their excitation function maxima and is the value adapted for the estimate of fusion probability above for  $^{54}\text{Cr} + ^{162}\text{Dy}$ .

In the search for superheavy elements near the island of stability and with reactions involving projectile heavier than  $^{48}\text{Ca}$ , the presently discussed effects are critical in determining experimental success. Although strong shell correction energies reduce the fissility of a nucleus, the collective excitation in weakly deformed nuclei is likely to cancel out this contribution and reduce survival of the residue. Even though the synthesis of element 120 is accompanied with these challenges and pushes the capabilities of modern instruments, it is not completely beyond reach as the record for lowest production cross section measured is purported to be 31 fb [12].

- [1] K. Siwek-Wilczynska, T. Cap, M. Kowal, A. Sobiczewski, and J. Wilczynski, *Phys. Rev. C* **86**, 014611 (2012).
- [2] V. Zagrebaev and W. Greiner, *Phys. Rev. C* **78**, 034610 (2008).
- [3] A. Sobiczewski and K. Pomorski, *Prog. Part. Nucl. Phys.* **58**, 292 (2007).
- [4] C.M. Folden III *et al.*, *Nucl. Instrum. Methods Phys. Res.* **A678**, 1 (2012).
- [5] D.A. Mayorov, M.C. Alfonso, T.A. Werke, and C.M. Folden III, *Progress in Research*, Cyclotron Institute, Texas A&M University (2010-2011), p. II-19.
- [6] V.I. Zagrebaev, Y. Aritomo, M.G. Itkis, Y.T. Oganessian, and M. Ohta, *Phys. Rev. C* **65**, 014607 (2001).
- [7] D. Vermeulen, H.G. Clerc, C.C. Sahm, K.H. Schmidt, J.G. Keller, G. Munzenberg, and W. Reisdorf, *Z. Phys. A.-Hadrons Nuclei* **318**, 157 (1984).
- [8] A.R. Junghans, M. de Jong, H.G. Clerc, A.V. Ignatyuk, G.A. Kudyaev, and K.H. Schmidt, *Nucl. Phys.* **A629**, 635 (1998).
- [9] V.I. Zagrebaev *et al.*, <http://nrv.jinr.ru/nrv/>.
- [10] K. Siwek-Wilczynska, A. Borowiec, I. Skwira-Chalot, and J. Wilczynski, *Int. J. Mod. Phys. E* **17**, 12 (2008).

- [11] C.C. Sahm, H.G. Clerc, K.H. Schmidt, W. Reisdorf, P. Armbruster, F.P. Hessberger, J.G. Keller, G. Münzenberg, and D. Vermeulen, Nucl. Phys. A **441**, 316 (1985).
- [12] K. Morita *et al.*, J. Phys. Soc. Japan. **76**, 045001 (2007).
- [13] P. Moller, J.R. Nix, W.D. Myers, and W.J. Swiatecki, At. Nucl. Data **59**, 185 (1995).
- [14] A.J. Sierk, Phys. Rev. C **33**, 2039 (1986).
- [15] National Nuclear Data Center (2011), <http://www.nndc.bnl.gov>.
- [16] K.H. Schmidt, C.C. Sahm, K. Pielenz, and H.G. Clerc, Z. Phys. A. **316**, 19 (1984).